Specialty Wood Products Research Partnership

UNIVERSITY OF CANTERBURY
Te Whare Wānanga o Waitaha
CHRISTCHURCH NEW ZEALAND

Technical Report

Assessing *paropsine* damage on *Eucalyptus* trees with remote sensing

Author/s: Leslie Mann, Justin Morgenroth, Cong (Vega) Xu, and Stephen Pawson

Date: 19th of September 2022

Report: SWP-T153

FOREST GROWERS RESEARCH

Table of Contents

supported by forestgrowers commodity levy

EXECUTIVE SUMMARY

New Zealand forests comprise 10.1 million hectares of forests. Due to the sheer scale of managing these forests, remote sensing is increasingly used as a source of information for decision-making. Information on tree growth, mortality, and health related to climate or pest activity can be monitored and quickly mapped. Currently, no remote sensing methods exist to quantify foliar browse by paropsine beetles on *Eucalyptus*. Currently, defoliation assessments are performed through visual methods by ground-based observers. Such methods, like the Crown Damage Index (CDI), are time-consuming, particularly at larger spatial scales, and potentially suffer from observer bias.

Paropsine damage does not induce a colour change in foliage as would occur with a leaf-sucking insect. Instead, paropsines reduce canopy density by eating parts of leaves, thus altering their shape and area. Hence, LiDAR could be a suitable tool for paropsine defoliation assessment. This study aimed to evaluate the potential for LiDAR as a quantitative assessment of paropsine defoliation of *Eucalyptus* crowns as a replacement for the CDI.

Three LiDAR scanners (VUX-240, VUX-1LR and L1) were used to collect data from a *Eucalyptus* trial in the Canterbury region (43°11'47.2"S 172°39'06.1"E) in September 2021 and March 2022. To measure the defoliation prediction accuracy of LiDAR we simultaneously collected CDI data for 55 tree crowns at the same date as the LiDAR data. A total of 57 LiDAR metrics were extracted for each of the 55 tree crowns. The best metrics model to predict CDI was statistically analysed with a Partial Least Squares Regression (PLSR).

Results:
The results demonstrated 18 LiDAR metrics of interest and showed that LiDAR scanners could predict CDI with ±19.1-23.6 % error from the actual CDI observed in the field, with VUX-240 having the smallest error prediction (Root Mean Square Error (RMSE)=9.5 CDI units in September 2021), followed by the L1 scanner (RMSE=10.5 CDI units in March 2022), and VUX-1LR having the highest error prediction (RMSE=11.8 CDI units in September 2021 and RMSE=11.6 CDI units in March 2022).

Key conclusions are:

- All three scanners had comparable predictive abilities, meaning that all could possibly be used for paropsine defoliation assessment.
- The actual error prediction shows promise as a healthy tree could be distinguished from a heavily defoliated tree.
- More testing needs to be undertaken to increase the LiDAR defoliation prediction accuracy. These tests should occur in sites with a broader CDI range (e.g., the Marlborough region).
- Future work needs to move away from the CDI and use a quantitative method of assessing crown defoliation that can be compared with the remotely sensed LiDAR data. This is important as the CDI is semi-quantitative and potentially subject to observer bias.
- More testing needs to be undertaken to determine whether LiDAR can differentiate between paropsine beetle defoliation and trees where abiotic stresses have led to small leaves and/or sparse crowns

INTRODUCTION

Remote sensing to assess insect defoliation on Eucalyptus

In 2022, forests covered 38% of New Zealand's land, representing a total of 10.1 million hectares. This includes 1.7 million hectares (8%) of productive plantation forests (*About New Zealand's forests*, 2022). Due to the sheer scale of managing these forests, remote sensing is increasingly used as a source of information for decision-making (Ye et al., 2021). Information on tree growth, mortality, and health related to climate or pest activity can be monitored and quickly mapped (Hall et al., 2006). Currently, there are no remote sensing methods to assess foliar browse by paropsine beetles on *Eucalyptus*; and most of these defoliation assessments are performed through ground-based visual assessment.

Lin (2017) used the Crown Damage Index (CDI), a visual assessment that was developed by Stone et al. (2003), to assess eucalypt defoliation. The CDI visually estimates individual leaf and total crown defoliation. Lin (2017) went further and counted the abundance of paropsine beetle defoliators (*Paropsisterna cloelia* and *Paropsis charybdis*) as a measure of pest impact. Mann and Pawson (2022) continued using the CDI method to assess the defoliation of different eucalypt species and more in-depth studies of *E. bosistoana* and *E. tricarpa* families at the Dillon and Lissaman NZDFI trial sites in Marlborough. Such ground-based observational methods are time-consuming, particularly at larger spatial scales. Although the CDI method has been validated by the State Forests of NSW, Forestry Tasmania and the Queensland Forestry Institute (Stone et al, 2003), it still suffers from potential observer bias and is only semi-quantitative. LiDAR or visual imagery taken from above canopy offers a potential solution to these problems by providing a faster assessment alternative, especially for larger trees or difficult-to-access areas (Rhodes et al., 2022; Senf et al., 2017; Silva et al., 2013).

A tree's canopy can change in various ways in response to different forest health issues. Change can manifest as a loss of foliage, as leaves are either eaten or abscised by the plant, which alters the canopy density (Béland et al., 2014). Alternatively, canopy density may not change, but a colour variation in response to pests or diseases may occur (Barnes et al., 2017). It is well known that plants' spectral wavelengths absorbed and reflected (including invisible wavelengths) change in response to stress (dos Santos et al., 2017). Chewing insects can affect tree light absorption and reflectance due to changes in leaf morphology and composition (Hall et al., 2006). Modifications in the canopy in response to herbivory can generally be visible from above the canopy. Thus, quantifying canopy defoliation from above may be possible if an appropriate sensing technique can detect changes in canopy density and/or colour.

There are many options to remotely sense a forest canopy; these can be divided into passive and active sensors. Passive sensors detect reflections from existing electromagnetic sources, e.g., the sun, and include multispectral imaging and hyperspectral imaging. Multispectral imaging comprises all sensors with more than two spectral bands, and hyperspectral imaging regroups sensors with hundreds of bands. Active sensors emit electromagnetic signals, then intercept them after they have reflected off of target objects. This includes Radio Detection and Ranging (RADAR) and Light Detection and Ranging (LiDAR). Interestingly, passive sensors can use photogrammetric approaches to yield 3D point clouds, much like the output of LiDAR. Both types of sensors can be deployed by satellites, piloted aircraft (planes and helicopters), or unpiloted aerial vehicles (UAVs) (*What is remote sensing? The definition guide*, 2021). The spatial resolution of the imagery is determined in part, by the proximity of the sensor to the target; hence low flying UAV can capture data at the highest spatial resolution, but piloted aircraft and satellites can capture data from a larger spatial extent.

PASSIVE SENSORS

Multispectral imagery

RGB imagery

Leidemer et al. (2022) used RGB imagery to define six categories of *Polygraphus proximus* (bark beetle) damage on tree forests *(Abies mariesii).* They compared the percentage of white pixels per tree to assess its health (1 is healthy, 6 is dead). The average precision was 62%, with category 1 reaching a precision of 73% and category 6 a precision of 93% when compared to visual assessment.

Near Infrared imagery added to the RGB imagery

The broader spectral range of a multispectral sensor includes a NIR band in addition to the RGB band and is frequently used to quantify plant stress (Mcfadyen et al., 2014). Plant stress identification is valuable because it can be used to calculate vegetation indices, which are often highly correlated to leaf biomass and health (Silva et al., 2013). Vegetation indices, like the "Normalised Difference Vegetation Index" (NDVI), are widely used in arable and pastoral systems. For example, Catorci et al. (2021) used NDVI to measure climate-induced stress in pastoral systems. Similarly, Falkenstrom et al.(2002) assessed slight and moderate stress defoliation on pine (*Pinus sylvestris*) and spruce (*Picea abies*) trees with NDVI. Results were promising, with a correlation coefficient between defoliation and NDVI of r=-0.73 to -0.91. Variation in model performance was tree species dependent with defoliation predicted most accurately for pine trees. A study from Dash et al.(2018) showed that herbicide stress on *Pinus radiata* could be detected by satellite imagery and by using UAV mounted sensors it could distinguish at the tree level. Changes in vegetation through time were detected with structural metrics, mostly with NDVI, RENDVI and GNDVI, with the same indices decreasing or decreasing for the UAV and satellite imagery data. The datasets relationship gave a model strength between satellite and UAV structural metrics of R^2=0.91 for RENDVI, R^2=0.84 for GNDVI and R^2=0.82 for NDVI. Goodbody et al. (2018) used RGB and NIR imagery photogrammetry to monitor changes in canopy health caused by *Choristoneura fumiferana* (spruce budworm) defoliation. They measured defoliation prediction by comparing ground-based defoliation assessment (here, called cumulative defoliation) with spectral (mean value of band, standard deviation of band, etc.) and structural (90^{th} percentile of height, skewness, kurtosis, etc.) metrics. The spectral metrics model was most accurate, predicting cumulative defoliation with R^2= 0.79, against R^2=0.49 for the structural model. The model combining spectral and structural metrics gave and R^2= 0.79. Cardil et al. (2017) used RGB and Lidar technology to assess the defoliation of pine trees by *Thaumetopea pityocampa* (pine processionary moth), achieving a classification accuracy of 79% (non-infested and infested). These results suggest that RGB imagery may be used to assess paropsine damage on *Eucalyptus* trees. Paropsine defoliation does not cause a specific colour change to the leaves, however the removal of foliage may create colour differences in the crown with a reduction of "green".

Hyperspectral imagery

Another passive sensor used to detect defoliation is hyperspectral technology. Fraser et al. (2005) investigated *Lambdina fiscellaria* (eastern hemlock looper) damage on coniferous forests with hyperspectral satellite imagery (VGT sensor). The results showed an accuracy of R^2= 0.97 (samples divided into defoliated and non-defoliated trees) for forest areas larger than 5-10 km^2. In this study, the forest was highly defoliated and homogenous. Despite this relatively simple environment, many false detections were observed. They concluded that improvements were needed to adapt the model to a more diverse and less defoliated forest. Nasi et al. (2015) used hyperspectral technology to assess *Ips typographus* L. (bark beetle) damage at the tree level. Single trees were detected with an accuracy of 74% and tree health (dead, infested, healthy) was sensed with a final accuracy of 76%. Another study from Abdel-Rahman et al. (2014) assessed *Sirex noctilio* damage on pine trees in South Africa. The study used hyperspectral imagery to classifying the results in three infestation phases, depending on the color (green, red and grey). Results showed an accuracy of 74.5% with the Forest classification and 73.5% for the Support Vector Machines classifiers. Hyperspectral imagery does not seem to be the most suitable remote sensing methodology for our experiment as a) it is expensive, and b) most available sensors have low spatial resolution making it more suitable for large scale analysis rather than individual tree crown analysis.

ACTIVE SENSORS

Radio Detection and Ranging (RADAR)

Bae et al. (2022) quantified *Lymantria dispar* (spongy moth) defoliation on mixed oak forests using satellite RADAR. A canopy development index was extracted from the RADAR data collected at the beginning and the end of the experiment. The RADAR effectiveness was verified by comparing the results with foliage estimates obtained using optical (sentinel-2), terrestrial laser scanning (TLS), also called terrestrial LiDAR, and pest counting. They demonstrated that RADAR data were correlated with the optical data (Spearman's p=0.79), TLS data (Spearman's p=0.84) and physical counts of spongy moths (R2=0.52). RADAR has also been used to detect *Ips typographus* (Eurasian spruce bark beetle) outbreaks (Hollaus & Vreugdenhil, 2019) and *Neodiprion sertifer* (European pine sawfly) on *Pinus sylvestris* (Scots pine) forests defoliation. Likewise, the effectiveness of RADAR in detecting European sawfly damage was assessed by comparing RADAR results with TLS data, a visual defoliation assessment method, and the tree structure (needles, stems and branches) (Kaasalainen et al., 2010). Results suggested that TLS and RADAR combined have the potential to detect canopy changes, with TLS being best at detecting changes in biomass.

Light Detection and Ranging (LiDAR)

LiDAR (sometimes referred to as Airborne Laser Scanning (ALS) (Roussel et al., 2020)) works by emitting pulsed laser waves that are reflected (a 'return') from objects in the environment. The time it takes each pulse to return to the laser is then used to calculate the distance between the laser the object. Hundreds of thousands of pulses are emitted per second with modern LiDAR and together, their returns form a dense point cloud (Béland et al., 2014). This point cloud can then be used to describe the characteristics of trees, including leaf area and canopy density, that are important for insect defoliation applications (Pearse et al., 2017). LiDAR systems can be described as either discrete returns or full waveform systems. A discrete system only captures part of the potential data cloud and is limited to a few tens of measurements. This system may include from one to five, sometimes more, returns from each pulse. The full waveform system considers the whole range of returns (could be more than hundreds) to register the light energy returned to the laser during a time period. The full waveform system is more complex to process, even though it can provide more information than the discrete system (Lim et al., 2003). Discrete return LiDAR remains the most convenient and widely-used LiDAR tool system in forestry for point cloud overview and several processing steps like the Digital Surface Model (DSM) and Canopy Height Model (CHM)(Lim et al., 2003).

LiDAR has been used extensively as a tool to quantify insect defoliation. Kruskamp et al. (2011) used LiDAR to detect the presence or absence of *Adelges tsugae* (hemlock woolly adelgid) in a Georgia National Forest. The study showed that hemlock tree health could be accurately categorize health in three categories (with 1 as healthy and 3 as unhealthy) with LiDAR data using LAI (R^2=0.73) and fractional cover (R^2=0.47) at cluster size (15-20 m). Meng et al. (2018) assessed LiDAR tools as defoliation predictors for *Lymantria dispar L.* (spongy moth) defoliation on mixed oak-pine forests. LiDAR metrics could detect variation in canopy structures with a R^2=0.77 and a RMSE =15.37%. A more recent study from Lin et al. (2019) showed that defoliation could be assessed by both hyperspectral imagery (R^2=0.67, RMSE=15.87%) and LiDAR (R^2=0.69, RMSE=12.28%), with better results obtained by LiDAR. Moreover, a combination of both sensors most accurately (R^2=0.83, RMSE=9.93%) assessed pine tree defoliation by *Tomicus spp.* (pine shoot beetle).

The widespread adoption of LiDAR for forest characterisation in New Zealand has been hindered by various barriers (Morgenroth & Visser, 2013). However, that is changing and now LiDAR is commonly applied to various forestry applications (De Gouw et al., 2020). Lower cost and new technologies, including affordable drones, allow broader use of the LiDAR-based applications (Béland et al., 2014). Remote sensing methods (data collection and processing) have various advantages and limitations. Choosing the right one will depend on the area and what should be monitored. The spatial, spectral and temporal resolution may substantially impact the final result. Data classifications in remote sensing, such as Maximum Likelihood classification (MLC), random Forest classification (RF), the Support Vector Machines classifiers (SVM), or the Classification and

Regression Tree (CART) may also have significant impacts (Belgiu & Drăguţ, 2016). Fortunately, new remote-sensing technologies allow cost-effective, tree-level assessments (Gu et al., 2020).

Remote sensing applied to the study

Paropsine damage does not induce a colour change in foliage like a leaf-sucking insect. Instead, paropsines reduce canopy density by eating parts of leaves, thus altering their shape and area. Hence, LiDAR could be a suitable tool for paropsine defoliation assessment. This study aimed to evaluate the potential of LiDAR as a quantitative method to assess paropsine defoliation of *Eucalyptus* crowns as a replacement for the subjective, time-consuming, Crown Damage Index. A well-established method to derive forest attributes from LiDAR is the area-based approach (ABA), where the study area is divided into a grid-cell structure (Roussel et al., 2020). This method depends on the structural metrics, which are then used to build the regression model. This technique allowed the model to be perfectly calibrated to the area, however each area surveyed requires model calibration prior to surveys (Coomes et al., 2017). This method may be suitable to assess defoliation per area without being tree specific or with a homogeneous forest. An alternative approach is based on individual tree segmentation (ITS) (Roussel et al., 2020). The ITS method is used to obtain tree top localisations and delineates tree crowns. LiDAR metrics (i.e., a statistical or quantitative description of the point cloud) are calculated for each tree crown or cell for the ITS and ABA scenarios, respectively (Roussel et al., 2020). This ITS method is more adapted to heterogenous forests as it could detect defoliation at tree level. Although ITS is more straightforward in obtaining information at the tree level, its application may be limited by a lack of point cloud density, inaccurate spatial location of trees and under detection of trees under the upper canopy (Coomes et al., 2017; Roussel et al., 2020). In this study, paropsine defoliation needed to be assessed at the tree level, and not per cell. Thus, the ITS method is most suited to this application. Many potentially relevant LiDAR metrics can be used to quantify attributes, such as tree height (Griffin et al., 2008; Roussel et al., 2020; St Peter et al., 2021), canopy cover (Griffin et al., 2008; Roussel et al., 2020; St Peter et al., 2021), biomass (Roussel et al., 2020), basal area (Roussel et al., 2020; St Peter et al., 2021) and leaf area index (LAI) (Griffin et al., 2008; Pearse et al., 2017).

The main metrics used to assess defoliation on trees are the 70th bincentile height, the intensity skewness, the intensity kurtosis (Meng et al., 2018), the 90th and 95th and 99th height percentile, the maximum height and skewness of height distribution (Goodbody et al., 2018; Vescovo et al., 2016). Because insect defoliation measurement with LiDAR is comparatively poorly understood, other metrics generally used in forestry may be significant. These include; kurtosis of height distribution, the mean height, the return fractions (Martins-Neto et al., 2021) (Table 1), the canopy cover, and the canopy density (Pearse et al., 2017). Nevertheless, single tree crown segmentation, delineation and the metrics related to tree defoliation remain a technological challenge (Gu et al., 2020) that foresters have only started to investigate. This project is the first step in evaluating LiDAR suitability to assess paropsine damage on *Eucalyptus* trees. If successful, such a method would be faster, and more consistent than ground-based visual assessments using the CDI, especially where a large number of trees need to be measured or terrain is challenging/inaccessible.

METHODS

Site and Eucalyptus trees

The *Eucalyptus* study site was located in Sefton, Canterbury region (43°11'47.2"S 172°39'06.1"E). Two *Eucalyptus* trials at this site were assessed with LiDAR. The first trial comprises trees from six species planted in 2011. This included *E. bosistoana*, *E. camaldulensis*, *E. cladocalyx*, *E. globoidea*, *E. tricarpa* and *E. quadrangulata* from the *Symphyomyrtus* subgenus, and *E. globoidea* from the *Eucalyptus* subgenus. The second trial comprised trees from different *E. bosistoana* families planted in 2010.

LiDAR data collect in the field

Data were collected twice to sample trees before and after the main paropsine activity period. The first sample was taken in September 2021, just before paropsines became active, and the second sample in March 2022. This permitted a comparison of LiDAR data collected for trees with little damage and trees subjected to greater levels of defoliation. In the middle of September, the data were collected with two different laser scanners to assess what data density was best to assess paropsine defoliation. The high-density scan was accomplished with a VUX-240 laser scanner (228 points per square meter) attached to a Europcoter EC120 Colibri helicopter. The low-density scan was from a VUX-1LR (20 points per square meter) attached to a Guimbal Cabri G2 helicopter. Both data sets were collected between the 13th and the 17th of September 2021. The second collection was done with the same VUX-1LR on 18th March, however the VUX-240 was unavailable as it was based in Antarctica at that time. Instead, a Livox LiDAR module (L1) attached to a UAV (DJI Matrice 300 RTK) was used that achieved point densities of 1509 points per square meter for the species trial and 1815 points per square meter for the *E. bosistoana* families trial on 1st March 2022.

Choosing the metrics

A total of 57 metrics (Table 1) were derived for each of the four point clouds (VUX-240, VUX-1LR September 2021 and March 2022, and L1).

Table 1: LiDAR metrics extracted from the segmented point cloud before sorting (Martins-Neto et al., 2021). Total of 57 metrics used to analyse the possible prediction of CDI.

Metrics extracted	Description
itot	sum of intensity for each return
imax	maximum intensity
imean	mean intensity
isd	standard deviation intensity
iskew	skewness of intensity distribution
ikurt	kurtosis of intensity distribution
ipcumzq x^{th}	percentage of intensity returned below the x^{th} (10, 30, 50, 70, 90) (bicentile)
zmax	maximum height
zwimean	mean elevation weighted by intensity
zimean	mean products of z by intensity
zmean	mean height
zsd	standard deviation of height distribution
zskew	skewness of height distribution
zkurt	kurtosis of height distribution
zsqmean	quadratic mean
zentropy	entropy of height distribution
pzabovemean	percentage of return above zmean
pzabove2	percentage of return above z 2 meter
pxth	x returns by pulses (1, 2, 3, 4, 5)
zq x^{th}	X^{th} percentile of height distribution (5, 10, 15, 20, 25, 30, 35, 40, 45, 50, 55, 60, 65, 70, 75, 80, 85, 90, 95)
zpcum x^{th}	cumulative percentage of return in the x^{th} layer (1-9) with f(z)

LiDAR workflow

The software commonly used for LiDAR data processing are LAStools, Whitebox GAT, FUSION, Laser-chicken, RLidar Package, lidR (St Peter et al., 2021). LAStools (Isenburg, 2012), R (lidR package) (Roussel et al., 2020) and ArcGIS were used to process the LiDAR data for this study. The raw LiDAR data were processed with DJI Tera software to obtain a LAS file. The LAS file was then further processed on Lastools. The LAStools commands lasnoise, lasground, lasheight, and lasclassify were used as a first step to clean the LiDAR point cloud. The noise was removed, the point cloud was classified (excluding points above 25 meters, classifying points below 0.2 meter as ground, points between 0.21 and 1 meter as low vegetation, and points from 1.1 to 18 meters as high vegetation) and normalized. R (RStudio interface, lidR package) was used to extract the Digital Surface Model (DSM) and Canopy Height Model (CHM) from the LASfile (Roussel et al., 2020). The DSM captures the shape of the earth's surface, including all natural and human structures (Marwaha & Duffy, 2021). The CHM is a high-resolution raster layer that can map structure elevations as a continuous surface (*Canopy Height Model (CHM)*, 2021). The CHM was created with a resolution of 0.5 m and a radius circle of 0.15 m. Finally, the CHM was visualised in ArcGIS and the crowns of all 55 trees with GPS coordinate were manually delineated. This manual delineation allowed a more precise individual tree crown for an optimal comparison CDI/metric predictors. This manual crown delineation was then uploaded in R and used to clip the LAS file to obtain one point cloud per tree. Then, 57 different metrics were extracted within each tree polygon (Table 1).

Crown damage Index (CDI) data

Crown defoliation was estimated using the CDI method. The CDI method is a visual defoliation estimate of the entire tree. A derivative of the CDI is the CDI shoot assessment that evaluates three shoots that are observed in detail as a substitute for a full tree crown assessment. This sampling technique is more practical with taller trees where a pole pruner allows sampling of upper crown shoots where paropsine beetle damage occurs. The CDI score is calculated as the (Incidence*Severity)/100. The incidence is the number of damaged leaves per shoot scored as an average from three shoots. The severity is the average level of damage per leaf, again averaged across three shoots (Christine Stone et al., 2003). This defoliation level measurement is the most common method used to assess *Eucalyptus* defoliation in Australia (Christine Stone et al., 2003; C Stone et al., 2003). Trials were assessed on 15th September to allow for comparison with the LiDAR data; 30 trees from the species trial (five per species) and 25 trees from the *E. bosistoana* trial were assessed. The coordinates of the 55 trees were recorded with a GPS (Geo7x handheld, Trimble Inc., New Zealand) so that trees could be collocated with trees delineated from the canopy height model. A second CDI measurement of the same 55 trees was performed at the end of the summer season (9th March 2022) to correlate ground measurements of CDI with the LiDAR metrics collected during the same period.

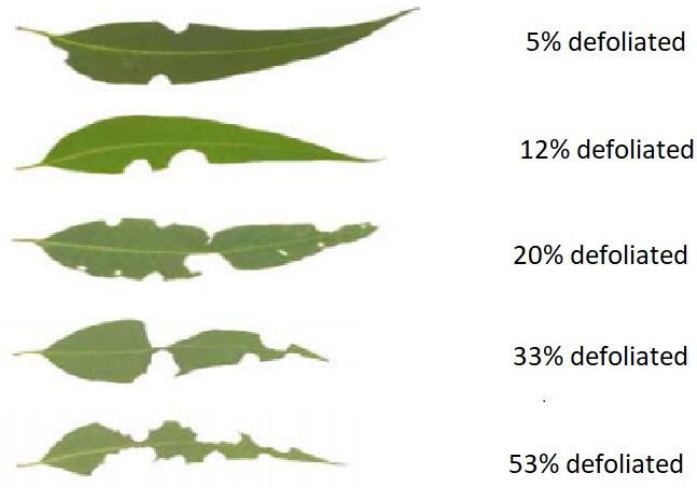

Image 1: Example of severity index for paropsine damage, Stone et al., 2003.

Statistical analysis

R (using R-studio interface) and Microsoft Excel were used for statistical analysis and data collection, respectively. We had a total of 57 LiDAR metrics for each of the 55 trees. A simple Pearson's correlation (rstatix package) was used to test the correlation between CDI and the different metrics (Table 1). Then, a second Pearson's correlation test using the corrplot package was used to test for multicollinearity between the 57 predictors. Due to possible multicollinearities and a high number of predictors, a Partial Least Squares Regression (PLSR), was used. A PLSR is similar to a Principal Components Analysis (PCA) and is commonly used in situations with small sample sizes and many possibly correlated predictor variables (Wehrens & Mevik, 2007). A multivariate PLSR approach is advantageous as it identifies multiple LiDAR metrics that, in combination, have better predictive power than a model based on a single LiDAR metric.

A PLSR was applied (package pls) to determine the optimal number of LiDAR metrics that best model the CDI. This method was used by Goodbody and al. (2018) to assess metrics that predict spruce budworm damage on trees. Best models were compared using the Root Mean Square Error of Prediction (RMSEP). The PLSR used a leave-one-out cross-validation (LOO) and 12 components. The 12 components were based on the convention that the maximum optimal number of predictors equals the number of samples/5. Thus, with 57 LiDAR metrics, our PLRS

model should have a maximum of 11 to 12 predictors. The effect of a linear transformation of the CDI variable was assessed on model performance. A prediction model fitting the PLSR model with the optimal number of predictors was evaluated using mean error (ME), mean absolute error (MAE), and root mean squared error (RMSE) tests. Finally, regression coefficients were extracted to quantify the percent variance explained by each metric. Tests were done separately for each collection of LiDAR data. The analysis with the L1 LiDAR was completed with only 43 trees rather than 55 due to a GPS error preventing the relocation of 12 trees in the dataset. The L1 PLSR analysis used only nine components in the LOO due to the reduced sample size.

When comparing the CDI with the LiDAR point clouds, the CDI was used as a percentage of defoliation damage. For modelling purposes, the response variable CDI needs to be transformed with a logistic regression (logit model) to facilitate normality and homoscedasticity of the residuals (Gasso, 2019).

RESULTS

VUX-240 LiDAR

Multicollinearity LiDAR metrics

A Pearson's correlation test was calculated between the different metrics for the VUX-240 to test multicollinearity. It showed that multicollinearities existed (Figure 1). In total, 1,485 metric correlations were tested for multicollinearity, from which 95 metrics correlations had a value above 0.95 (Table 1a appendices). This result demonstrates that metrics must be removed by performing a dimension reduction technique (e.g., PLSR) to avoid biases.

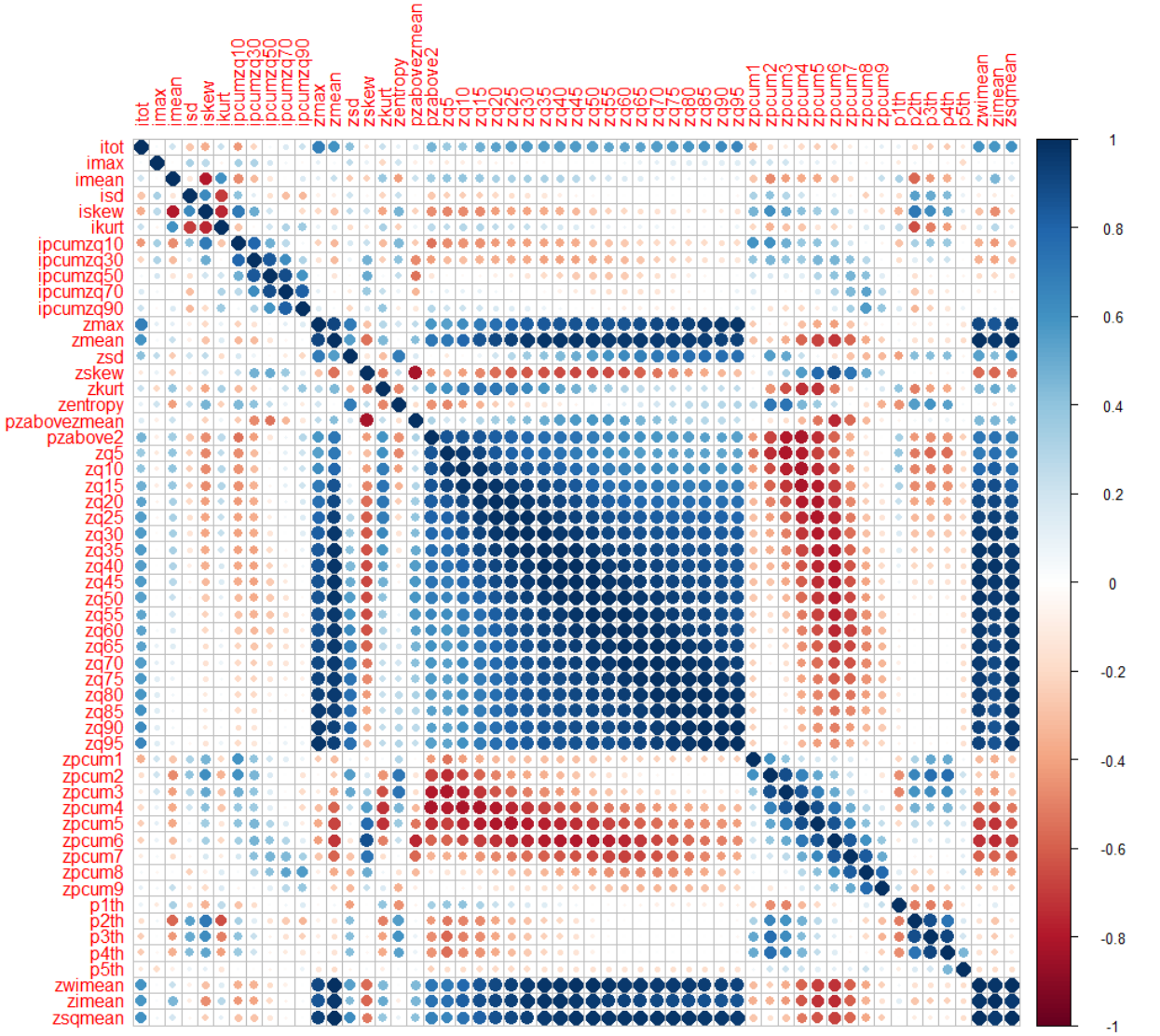

Figure 1: Matrix correlation of the 57 different metrics for the VUX-240 LiDAR scanner in September 2021. Many metrics were highly correlated (model with multicollinearity), with 95 metric correlations above 0.95.

CDI modelling with Partial Least Squares Linear Regression (PLSR)

The RMSEP extracted from the PLSR for the VUX-240 data (September 2021) demonstrated a model containing nine metrics (CV=1.093) performed best for predicting CDI (Figure 2). The predicted model run with nine metrics was linear (Figure 2), with a ME of 1.581, MAE of 7.118, and RMSE of 9.554 (Table 3). The RMSE*2 can be interpreted as the standard deviation of the predicted residual, meaning that 95% of the CDI predictions are expected to be within ± 19.1 of the true observed CDI for the VUX-240. The predicted model was linear, and the correlation of the measured CDI with the predicted CDI from the best model was r=0.64. The nine metrics used for the model could integrate different combinations of component metrics, as illustrated in Table 2.

The model with the logit transformation induced a slight mean error (ME of 1.58). Examining the predictive ability of LiDAR metrics without the logistic transformation (logit) automatically removed the mean error from our estimate. Without the logit, the best PLSR model had five LiDAR metrics. The predicted model with five metrics had a mean error of zero, MAE of 8.066, and an RMSE of 9.376 (Table 3). The correlation between the CDI and the predicted model with five metrics was 0.55. This correlation was weaker than in the model with the logit transformation.

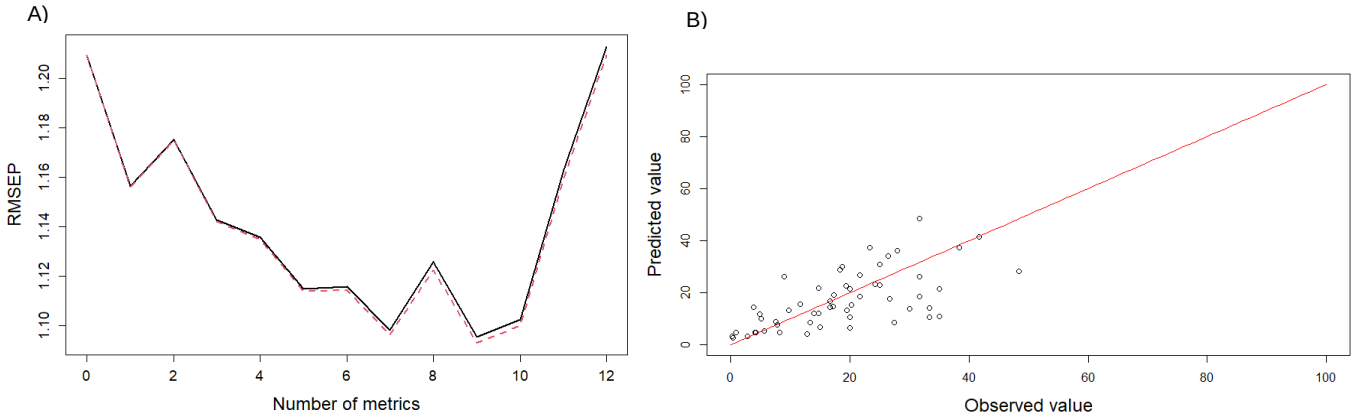

Figure 2: A) RMSEP extracted from the PLSR model with a linear transformation for the VUX-240 scanner in September 2021. Nine (CV=1.093) metrics were the best model to predict CDI. The black line represents the ordinary cross-validation estimate (CV). The red dashed line represents the bias-corrected CV estimate (adjCV). AdjCV varies depending on the validation method used. When a "Leave on out" method (LOO) is used, there is no difference between CV and adjCV. B) Linear regression of the predicted values against the observed values for the VUX-240 scanner.

Table 2: Weight of each variable in each linear combination with the predicting model with a linear transformation (nine metrics) for the VUX-240 scanner. The itot metrics will be the first metrics to use, followed by zimean. The third one could be imax, imean or zimean, etc. The metrics with no observed weight were removed from the table.

	Comp1	Comp2	Comp3	Comp4	Comp5	Comp6	Comp7	Comp8	Comp9
itot	-1.000								
imax			0.858	-0.793	0.173				
imean			0.449	0.827	-0.463				
isd					0.870				
pzabovezmean						-0.165	0.171	0.177	
pzabove2						-0.147	-0.241	0.240	-0.154
zpcum2								-0.117	
zpcum3						0.214	0.204	-0.281	0.224
zpcum4						0.385	0.191	-0.372	0.196
zpcum5						0.543	0.112	-0.327	0.195
zpcum6						0.545	-0.322	-0.162	0.163
zpcum7						0.461	-0.766		
zpcum8						0.481	-0.689	0.544	
zpcum9						0.234	-0.137	0.586	
p1th						0.341		0.323	-1.052
p2th								-0.478	0.123
p3th								-0.138	
zimean		-1.098	0.402						

Table 3: Mean Error (ME), MAE, RMSE, CDI and predicted CDI correlation, best number of metrics chosen and CV value (from PLSR model) for each LiDAR data clouds depending on the scanner type. Three scanners: VUX-240, VUX-1LR and Matrice 300. Data collected between the 13th and the 17th of September 2021 for VUX-240 and VUX-1LR. Data was collected on 1st March for Matrice300 and 18th March for VUX-1LR. 55 trees were sampled for VUX-240 and VUX-1LR. 43 trees were sampled for M300.

	Date	Scanner	ME	MAE	RMSE	Corr. CDI/predict	No metrics	CV	2*RMSE
CDI % (Logit)	Sept. 2021	VUX-240	1.581	7.118	9.554	0.638	9	1.095	19.109
	Sept. 2021	VUX-1LR	3.146	8.502	11.810	0.310	4	1.165	23.620
	March 2022	L1	2.911	8.024	10.515	0.460	2	1.079	21.030
	March 2022	VUX-1LR	3.651	9.168	11.624	0.473	4	1.369	23.248
CDI (non-transformed)	Sept. 2021	VUX-240	0.000	8.066	9.376	0.556	5	10.480	18.752
	Sept. 2021	VUX-1LR	0.000	7.845	10.191	0.428	4	11.650	20.382
	March 2022	L1	0.000	7.869	10.041	0.461	2	11.090	20.082
	March 2022	VUX-1LR	0.000	8.622	10.364	0.514	4	11.810	20.728

VUX-1LR LiDAR

Multicollinearity LiDAR metrics

September 2022

A Pearson's correlation test was calculated between the different metrics for the VUX-1LR to test multicollinearity. It showed that multicollinearities existed (Figure 1a appendices). Due to a lack of point density or missing data, metrics like zq5 to zq50, p4t and p5th were returning to zero for all samples (see "?" in figure 1a appendices). Zq55 to 85, and p3th had many samples returning to zero. Results for these metrics should be handled with care. In total, 903 metric correlations were tested, from which 33 metrics correlations had a value above 0.95 (Table 2a). This result demonstrates many metrics need to be removed by performing a dimension reduction technique to avoid biases.

March 2022

A Pearson's correlation test was calculated between the different metrics for the VUX-1LR to test multicollinearity. It showed that multicollinearities existed (Figure 2a appendices). Due to a lack of point density or missing data, metrics like zq5 to zq50, p4t and p5th returned zero values for all samples (labelled as "?" in figure 2a appendices). Zq55 to 85, and p3th had many samples returning to zero. Results for these metrics should be handled with care. In total, 903 metrics were tested, from which 33 metric correlations had a value above 0.95 (Table 3a). This result demonstrates many metrics need to be removed by performing a dimension reduction technique to avoid biases.

CDI modelling with Partial Least Squares Linear Regression (PLSR)

September 2022

The PLSR results obtained with the VUX-1LR scanner from September 2021 gave a ME of 3.146, a MAE of 8.502 and a RMSE of 11.810 (Table 3) for four metrics as the best model (Figure 3), meaning that this scanner could predict the CDI with ± 23.6 of the observed value. The correlation between the CDI and the predicted CDI was 0.31 (Table 3). The four best metrics to use for the CDI prediction were itot, zimean, a combination of imax, imean, isd and zimean and a combination of imax, imean and isd (Table 4).

The model with the logit transformation induced a mean error of 3.15. Examining the predictive ability of LiDAR metrics without the logistic transformation (logit) automatically removed the mean error to our estimate. Without the logit, the best PLSR model had four LiDAR metrics. The predicted model with four metrics had a mean error of zero, MAE of 7.845, and an RMSE of 10.191 (Table 3). The correlation between the CDI and the predicted model with five metrics was 0.43. This correlation was stronger than in the model with the logit transformation.

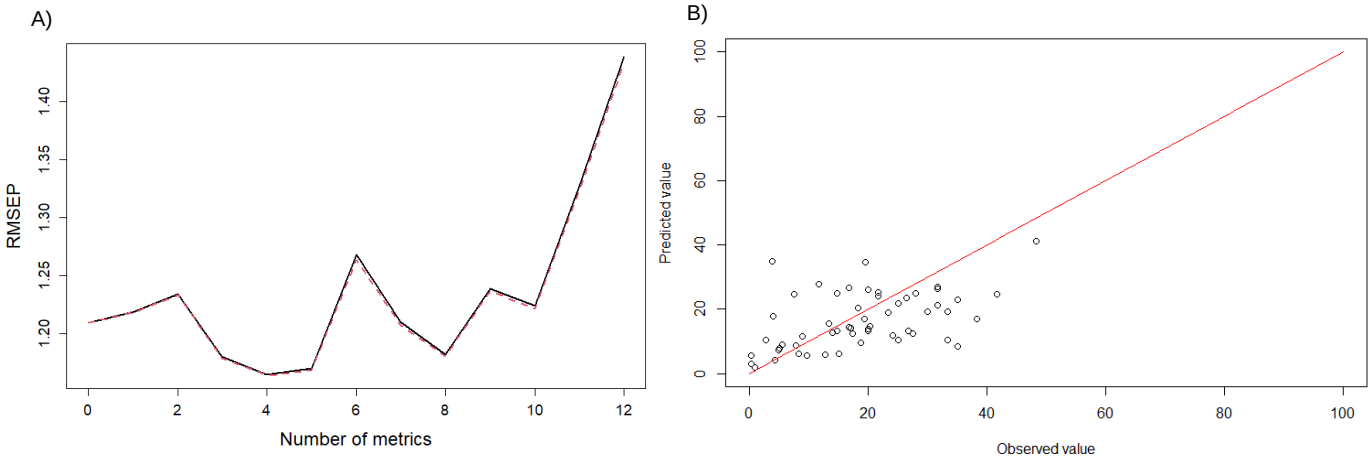

Figure 3: A) RMSEP extracted from the PLSR model with a linear transformation for the VUX-1LR scanner from September 2021. Four metrics (CV=1.165) were the best model to predict CDI. B) Linear regression of the predicted values against the observed one for the VUX-1LR scanner from September 2021. The regression is linear.

Table 4: Weight of each variable in each linear combination with the predicting model with a linear transformation (four metrics) for the VUX-1LR scanner from September 2021. The best metrics to use were itot, imax, imean, isd and zimean). The metrics with no observed weight were removed from the table.

	Comp 1	Comp 2	Comp 3	Comp 4
itot	-1.000			
imax			-0.352	-0.630
imean			0.857	-0.791
isd			-0.471	-0.301
zimean		-1.004		
0.136				

March 2022

The transformed PLSR results obtained with the VUX-1LR scanner from March 2022 demonstrated that four metrics were still the best model for this scanner (Figure 4). It produced a ME of 3.651, a MAE of 9.168 and a RMSE of 11.624 (Table 3), meaning that this scanner could predict the CDI with ± 23.2 of the observed value. The correlation between the CDI and the predicted CDI was 0.473. The four best metrics to use for the CDI prediction were itot for the first metric, zimean for the second one, a combination of imax, imean, isd and zimean for the third metric and a combination of imax, imean and isd for the fourth metric (Table 5).

The model with the logit transformation induced a mean error of 3.65. Examining the predictive ability of LiDAR metrics without the logistic transformation (logit) automatically removed the mean error to our estimate. Without the logit, the best PLSR model had four LiDAR metrics. The predicted model with four metrics had a mean error of zero, MAE of 8.622, and an RMSE of 10.364 (Table 3). The correlation between the CDI and the predicted model with five metrics was 0.51. This correlation was stronger than in the model with the logit transformation. Livox L1 LiDAR module

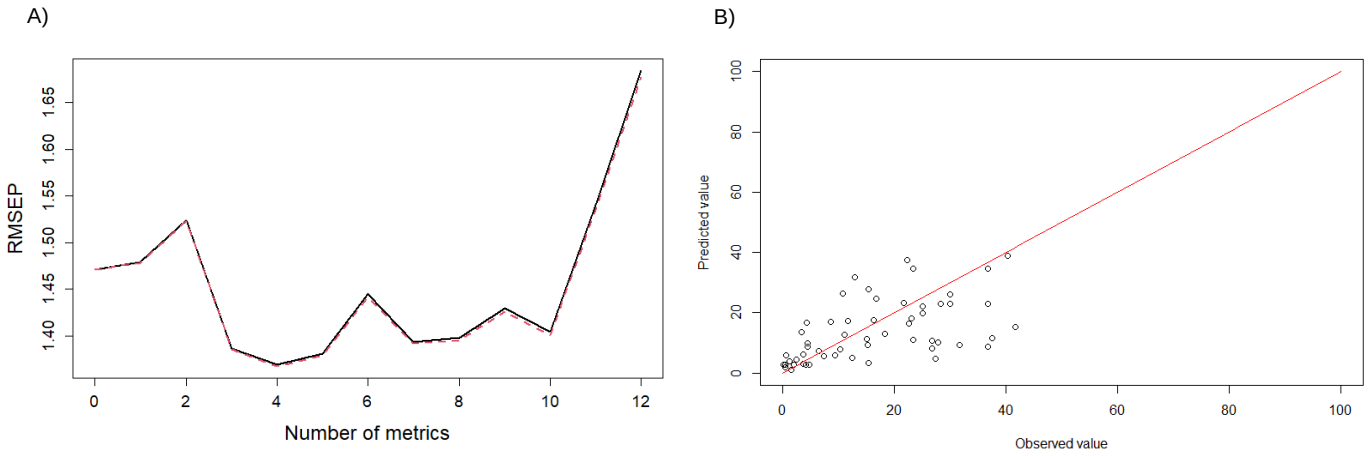

Figure 4: A) RMSEP extracted from the PLSR model with a linear transformation for the VUX-1LR scanner from March 2022. Four metrics (CV=1.369) were still the best model to predict CDI. B) Linear regression of the predicted values against the observed one for the VUX-1LR scanner from March 2022. The regression is linear.

Table 5: Weight of each variable in each linear combination with the predicting model with a linear transformation (four metrics) for the VUX-1LR scanner from March 2022. The best metrics to use were itot, imax, imean, isd and zimean). The metrics with no observed weight were removed from the table.

	Comp 1	Comp 2	Comp 3	Comp 4
itot	1.000			
imax			-0.166	-0.740
imean			0.920	-0.616
isd			-0.378	-0.433 -
zimean		-1.023	0.252	

L1 LiDAR

Multicollinearity LiDAR metrics

A Pearson's correlation test was calculated between the different metrics for the L1 scanner to test multicollinearity. It showed that multicollinearities existed (Figure 3a). Due to missing tree data (use of 43 trees rather than 55), metrics like zq5 to zq20, p3th to p5th had many samples returning to zero. Results for these metrics should be handled with care. In total, 1378 metric correlations were tested, from which 54 metrics correlations had a value above 0.95 (Table 4a). This result demonstrates many metrics need to be removed by performing a dimension reduction technique to avoid biases.

CDI modelling with Partial Least Squares Linear Regression (PLSR)

The transformed PLSR results obtained with the Livox L1 scanner from March 2022 demonstrated that the best model to predict CDI should include only two metrics (Figure 5). The ME was 2.91, the MAE 8.024 and the RMSE 10.515 (Table 3). With this scanner, the model could predict CDI with ±21% of the observed CDI. The correlation between the CDI and the predicted CDI was 0.46. The two best components to predict the CDI for this scanner are itot for the first component and a combination of imax, ipcumzq10, 30, 50 and 70, zkurt, pzabovemean, pzabove2, p1th, p2th and zimean for the second component (Table 6).

The model with the logit transformation induced a mean error of 2.91. Examining the predictive ability of LiDAR metrics without the logistic transformation (logit) automatically removed the mean error to our estimate. Without the logit, the best PLSR model had four LiDAR metrics. The predicted model with four metrics had a mean error of zero, MAE of 7.869, and an RMSE of 10.041 (Table 6). The correlation between the CDI and the predicted model with five metrics was 0.46. This correlation was similar to the model with the logit transformation.

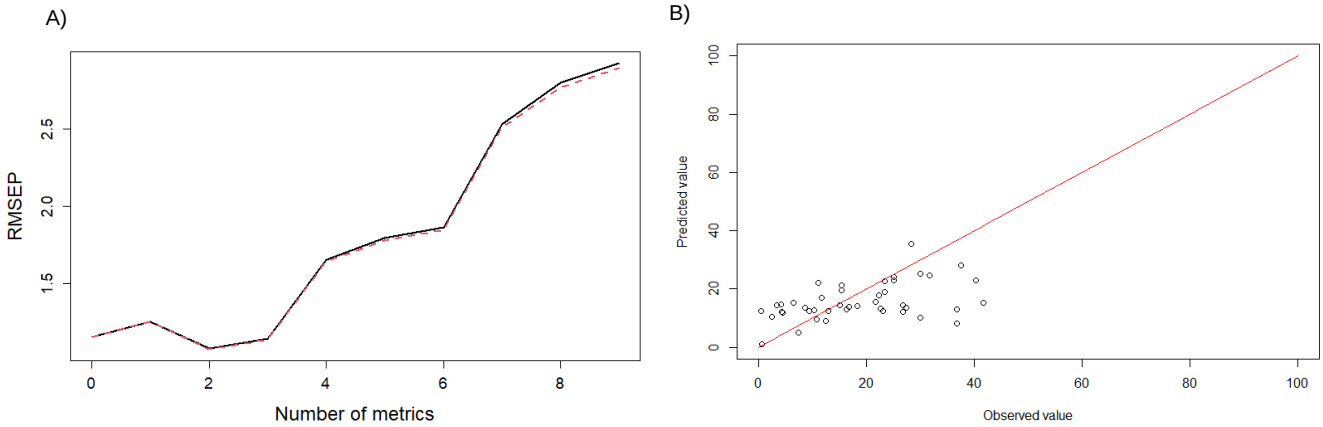

Figure 5: A) RMSEP extracted from the PLSR model with a linear transformation for the L1 scanner from March 2022. Two metrics (CV=1.079) were the best model to predict CDI.B) Linear regression of the predicted values against the observed one for the L1 scanner from March 2022. The regression is linear.

Table 6: Weight of each variable in each linear combination with the predicting model with a linear transformation (two metrics) for the L1 scanner from March 2022. The best metrics to use were itot for the first metric and a combination of imax, ipcumzq10, ipcumzq30, ipcumzq50, ipcumzq70, zkurt, pzabovezmean, pzabove2, p1th, p2th and zimean for the second metric). The metrics with no observed weight were removed from the table.

	Comp 1	Comp 2
itot	1.000	
imax		0.128
ipcumzq10		-0.234
ipcumzq30		-0.219
ipcumzq50		-0.163
ipcumzq70		-0.104
zkurt		-0.425
pzabovezmean		0.139
pzabove2		0.173
p1th		0.152
p2th		-0.117
zimean		0.785

LiDAR scanners comparison

Differences in CDI prediction for the VUX-1LR between September 2021 (±23.62%) and March 2022 (±23.25%) showed that the accuracy prediction stayed the same between seasons for this scanner. The correlation between CDI and predicted CDI increased through the season (0.473 in March 2022 against 0.31 in September 2021). There were multicollinearities with the metrics within the three LiDAR data scanners, with both VUX-240 and VUX-1LR from September 2021 having 95 metric correlations above 0.95. VUX-1LR and L1 from March 2022 had only 33 and 54 metrics correlation over 0.95, respectively.

The mean average difference between the observed actual CDI value and the predicted CDI value obtained from the LiDAR data was the lowest for the VUX-240 scanner (19.1%). Then, the L1 had a

mean average difference of 21%, and VUX-1LR had an average mean difference of 23.6% in September 2021 and 23.3% in March 2022. As these results refer to CDI as a percentage, a difference of approximately 5% between the scanners is minimal, especially between the VUX-240 and L1 scanners (a difference of only 2%). Even though the predicted CDI result was pretty similar for all LiDAR datasets, the metrics numbers (between 2 and 9) and the correlation between the CDI and the predicted CDI (r= 0.31 to r=0.64) varied substantially. The LiDAR scanners that were the most accurate so far were the VUX-240 and the L1 LiDAR. These LiDAR scanners had a denser point cloud compared to the VUX-1LR point cloud (only 19.87 points per m^2 against 227.91 and 1508.93 points per m^2 for the VUX-240 and L1 LiDAR, respectively), likely explaining their higher prediction accuracy. Our results suggest the accuracy of defoliation predictions will increase with point cloud density, which is to be expected. The L1 scanner had the highest point density, however its accuracy was lower than the VUX-240 scanner. This lower accuracy could be due to missing data (analysis done with 43 trees rather than 55 trees) and using a phone GPS rather than an RTK base for the L1 scanner.

Considering the price involved in using the VUX-240 and VUX-1LR (LiDAR price, helicopter use and competent staff hiring), the L1 LiDAR presents a more affordable solution, being attached to a UAV. Using the L1 on a UAV is suitable for assessing small forest areas like the NZDFI trials, especially if the trials need to be surveyed several times a year. If larger spatial scales need to be monitored, e.g., 100 ha+, aeroplane or helicopter would likely become more efficient.

Because the RMSE of both models (with and without the logit transformation) for every scanner had a similar enough RMSE for our analysis, both models could be used for the CDI prediction. For further analysis, the logit model only will be chosen.

Limitations of the experiment

During the LiDAR test experiment with the three different scanners, four main limitations appeared that could explain the weak accuracy prediction of the model.

1. The range in observed CDI values at the Sefton site did not cover the whole CDI scale (Figure 4). Maximum CDI values at the Martin site were at 50 CDI units, whereas in Marlborough, CDI values reached up to 80 (Figure 4). Hence, stronger correlations may have been identified if a greater range of CDI was available. A low infestation, coupled with the absence of EVB, more voracious than *P. charybdis,* was probably responsible for this low defoliation rate.
2. Only 55 trees were assessed for this first LiDAR experiment. Most remote-sensing studies used at least a few hundred trees to obtain a more robust statistical analysis (Leidemer et al., 2022).
3. The VUX-1LR defoliation comparison between September 2021 and March 2022 may have been masked by the high six months growth. Indeed, this period is when paropsines are the most active, but it is when the trees are growing the most too. In case of a low infestation, like in the Sefton site, the growth may have more impact than the paropsine defoliation.
4. The CDI method is semi-quantitative, involving a visual assessment. Our use of CDI was the first step to evaluating the ability of LiDAR to detect changes in canopy health due to paropsine defoliation. Hence, future extensions of this work need to develop quantitative measures of defoliation, e.g., using a leaf area scanner of individual trees to compare with the remotely sensed data.

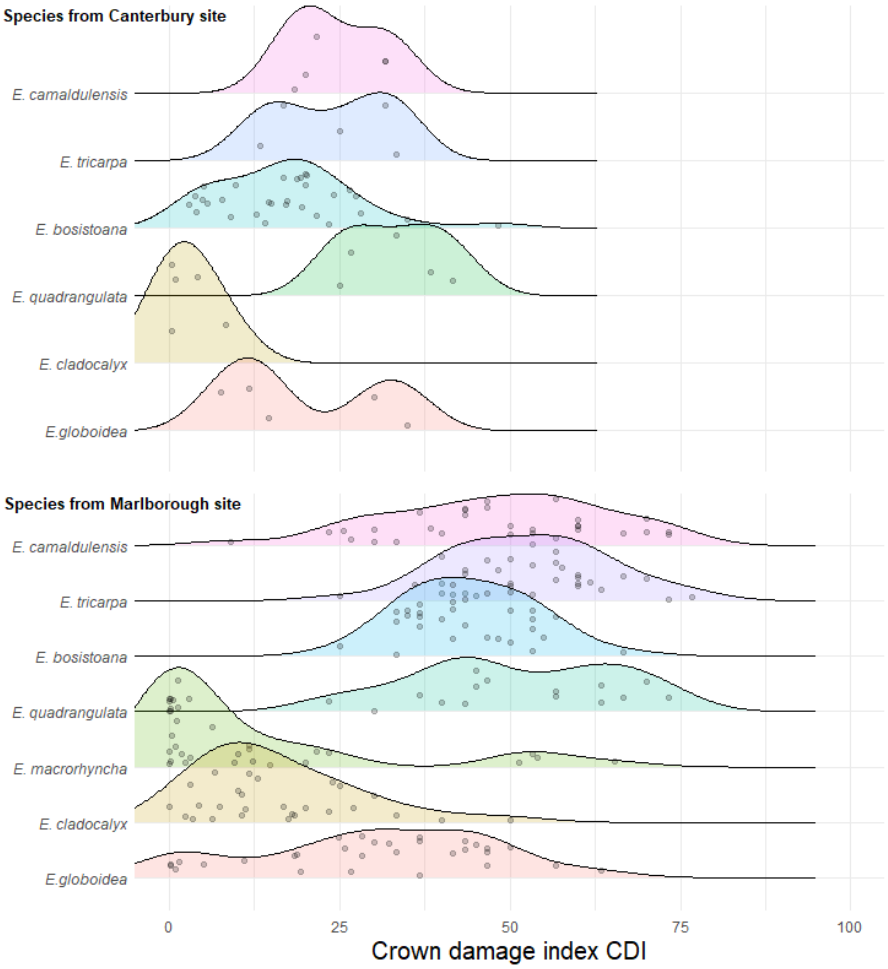

Figure 3: The different CDI frequency ranges of the Canterbury site (Sefton) used in this experiment and a Marlborough site. The Marlborough site is much more defoliated, with a CDI reaching up to 80 against a maximum of 50 for the Canterbury site.

CONCLUSION

Using LiDAR technology to assess paropsine defoliation shows promise. The LiDAR with the smallest prediction error was the VUX-240 scanner, followed by the L1 and finally the VUX-1LR (defoliation prediction was at ±19.1%, ±21% and ±23% from the observed CDI, respectively); This 5% accuracy difference between the three scanners showed that all could be as good tool to predict paropsine defoliation. However, using a LiDAR scanner attached to a drone rather than a helicopter seems to be the best lower-cost option to collect data from small trials like the NZDFI ones. To improve the model prediction accuracy, further experiments need to conducted at sites with a broader defoliation range, e.g., Marlborough region, and to develop a quantitative method to assess defoliation on individual trees to compare with the remote sensing data.
Finally, RBG data collected at the same time as the LiDAR data in March could be analysed and potentially combined with the LiDAR data to increase prediction accuracy (see introduction “Near Infrared imagery added to the RGB imagery”).

ACKNOWLEDGEMENTS

Funding: Specialty Wood Products (SWP) in Partnership with New Zealand Dryland Forest Initiative (NZDFI), New Zealand Institute of Forestry (NZIF), School of Forestry (that purchased some LiDAR data) and Entomological Society of New Zealand (ESNZ).

Collaborators: Elena Moltchanova (UC), Paul Millen (NZDFI), Josh McCulloch (UC), Kelvin Barsdale (UC), James Brasington (UC), Robyn Patient (UC).

Supervision: Stephen Pawson, Justin Morgenroth.

REFERENCES

Abdel-Rahman, E. M., Mutanga, O., Adam, E., & Ismail, R. (2014). Detecting *Sirex noctilio grey*-attacked and lightning-struck pine trees using airborne hyperspectral data, random forest and support vector machines classifiers. *ISPRS journal of photogrammetry and remote sensing, 88*, 48-59.

About New Zealand's forests. (2022, 05.05.22). New Zealand Forest Service. Retrieved 21.06.22, 2022, from https://www.mpi.govt.nz/forestry/new-zealand-forests-forest-industry/about-new-zealands-forests/

Bae, S., Müller, J., Förster, B., Hilmers, T., Hochrein, S., Jacobs, M., Leroy, B. M., Pretzsch, H., Weisser, W. W., & Mitesser, O. (2022). Tracking the temporal dynamics of insect defoliation by high-resolution radar satellite data. *Methods in Ecology and Evolution, 13*(1), 121-132.

Barnes, C., Balzter, H., Barrett, K., Eddy, J., Milner, S., & Suárez, J. C. (2017). Airborne laser scanning and tree crown fragmentation metrics for the assessment of *Phytophthora ramorum* infected larch forest stands. *Forest Ecology and Management, 404*, 294-305.

Béland, M., Baldocchi, D. D., Widlowski, J.-L., Fournier, R. A., & Verstraete, M. M. (2014). On seeing the wood from the leaves and the role of voxel size in determining leaf area distribution of forests with terrestrial LiDAR. *Agricultural and Forest Meteorology, 184*, 82-97.

Belgiu, M., & Drăguţ, L. (2016). Random forest in remote sensing: A review of applications and future directions. *ISPRS journal of photogrammetry and remote sensing, 114*, 24-31.

Canopy Height Model (CHM). (2021). Earth Define. Retrieved 22.07.22, 2022, from https://www.earthdefine.com/chm/

Cardil, A., Vepakomma, U., & Brotons, L. (2017). Assessing pine processionary moth defoliation using unmanned aerial systems. *Forests, 8*(10), 402.

Catorci, A., Lulli, R., Malatesta, L., Tavoloni, M., & Tardella, F. M. (2021). How the interplay between management and interannual climatic variability influences the NDVI variation in a sub-Mediterranean pastoral system: Insight into sustainable grassland use under climate change. *Agriculture, Ecosystems & Environment, 314*, 107372.

Coomes, D. A., Dalponte, M., Jucker, T., Asner, G. P., Banin, L. F., Burslem, D. F., Lewis, S. L., Nilus, R., Phillips, O. L., & Phua, M.-H. (2017). Area-based vs tree-centric approaches to mapping forest carbon in Southeast Asian forests from airborne laser scanning data. *Remote Sensing of Environment, 194*, 77-88.

Dash, J., Pearse, G., & Watt, M. (2018). UAV multispectral imagery can complement satellite data for monitoring forest health. *Remote Sensing, 10*(8), 1216.

De Gouw, S., Morgenroth, J., & Xu, C. (2020). An updated survey on the use of geospatial technologies in New Zealand's plantation forestry sector. *New Zealand Journal of Forestry Science, 50*.

dos Santos, A., Oumar, Z., Arnhold, A., da Silva, N., Oliveira Silva, C., & Zanetti, R. (2017). Multispectral characterization, prediction and mapping of *Thaumastocoris peregrinus* (Hemiptera: Thamascoridae) attack in *Eucalyptus* plantations using remote sensing. *Journal of Spatial Science, 62*(1), 127-137.

Falkenström, H., & Ekstrand, S. (2002). Evaluation of IRS-1c LISS-3 satellite data for defoliation assessment on Norway spruce and Scots pine. *Remote Sensing of Environment, 82*(2-3), 208-223.

Fraser, R., & Latifovic, R. (2005). Mapping insect-induced tree defoliation and mortality using coarse spatial resolution satellite imagery. *International Journal of Remote Sensing, 26*(1), 193-200.

Gasso, G. (2019). Logistic regression

Goodbody, T. R., Coops, N. C., Hermosilla, T., Tompalski, P., McCartney, G., & MacLean, D. A. (2018). Digital aerial photogrammetry for assessing cumulative spruce budworm defoliation and enhancing forest inventories at a landscape-level. *ISPRS journal of photogrammetry and remote sensing, 142*, 1-11.

Griffin, A. M., Popescu, S. C., & Zhao, K. (2008). Using LIDAR and normalized difference vegetation index to remotely determine LAI and percent canopy cover. *Proceedings of SilviLaser, 2008*, 8th.

Gu, J., Grybas, H., & Congalton, R. G. (2020). Individual tree crown delineation from UAS imagery based on region growing and growth space considerations. *Remote Sensing, 12*(15), 2363.

Hall, R. J., Skakun, R. S., & Arsenault, E. J. (2006). Remotely sensed data in the mapping of insect defoliation. *Understanding forest disturbance and spatial pattern: Remote sensing and GIS approaches*, 85-111.

Hollaus, M., & Vreugdenhil, M. (2019). Radar satellite imagery for detecting bark beetle outbreaks in forests. *Current Forestry Reports, 5*(4), 240-250.

Isenburg, M. (2012). LAStools—Efficient tools for LiDAR processing. *Available at: http: http://www. cs. unc. edu/~ isenburg/lastools/[Accessed October 9, 2012]*.

Kaasalainen, S., Hyyppä, J., Karjalainen, M., Krooks, A., Lyytikäinen-Saarenmaa, P., Holopainen, M., & Jaakkola, A. (2010). *Comparison of terrestrial laser scanner and synthetic aperture radar data in the study of forest defoliation* ISPRS Technical Commission VII

Thematic Processing, Modeling and Analysis of Remotely Sensed Data

Vienna, Austria.

Kruskamp, N. (2011). *LiDAR detection of defoliation in eastern hemlock due to hemlock woolly adelgid* [University of Georgia].

Leidemer, T., Gonroudobou, O. B. H., Nguyen, H. T., Ferracini, C., Burkhard, B., Diez, Y., & Lopez Caceres, M. L. (2022). Classifying the degree of bark beetle-induced damage on fir (*Abies mariesii*) forests, from UAV-acquired RGB images. *Computation, 10*(4), 63.

Lim, K., Treitz, P., Wulder, M., St-Onge, B., & Flood, M. (2003). LiDAR remote sensing of forest structure. *Progress in physical geography, 27*(1), 88-106.

Lin, H., Murray, T., & Mason, E. (2017). Incidence of and defoliation by a newly introduced pest, *Paropsisterna variicollis* (Coleoptera: Chrysomelidae), on eleven durable *Eucalyptus* species in Hawke's Bay, New Zealand. *New Zealand Plant Protection, 70*, 45-51.

Lin, Q., Huang, H., Wang, J., Huang, K., & Liu, Y. (2019). Detection of pine shoot beetle (PSB) stress on pine forests at individual tree level using UAV-based hyperspectral imagery and lidar. *Remote Sensing, 11*(21), 2540.

Mann, L., & Stephen, P. (2022). *Eucalyptus resistance to paropsine beetles*. University of Canterbury.

Martins-Neto, R. P., Tommaselli, A. M. G., Imai, N. N., David, H. C., Miltiadou, M., & Honkavaara, E. (2021). Identification of significative LiDAR metrics and comparison of machine learning approaches for estimating stand and diversity variables in heterogeneous Brazilian Atlantic forest. *Remote Sensing, 13*(13), 2444.

Marwaha, N., & Duffy, E. (2021). *Everything you need to know about Digital Elevation Models (DEMs), Digital Surface Models (DSMs), and Digital Terrain Models (DTMs)*. UP42. Retrieved 22.07.22, 2022, from https://up42.com/blog/tech/everything-you-need-to-know-about-digital-elevation-models-dem-digital

Mcfadyen, A., Gonzalez, L. F., Campbell, D. A., & Eagling, D. (2014). *Evaluating unmanned aircraft systems for deployment in plant biosecurity*. "Australian Research Centre for Aerospace Automation; School of Electrical Engineering & Computer Science; Science & Engineering Faculty".

Meng, R., Dennison, P. E., Zhao, F., Shendryk, I., Rickert, A., Hanavan, R. P., Cook, B. D., & Serbin, S. P. (2018). Mapping canopy defoliation by herbivorous insects at the individual tree level using bi-temporal airborne imaging spectroscopy and LiDAR measurements. *Remote Sensing of Environment, 215*, 170-183.

Morgenroth, J., & Visser, R. (2013). Uptake and barriers to the use of geospatial technologies in forest management. *New Zealand Journal of Forestry Science, 43*(1), 1-9.

Näsi, R., Honkavaara, E., Lyytikäinen-Saarenmaa, P., Blomqvist, M., Litkey, P., Hakala, T., Viljanen, N., Kantola, T., Tanhuanpää, T., & Holopainen, M. (2015). Using UAV-based photogrammetry and hyperspectral imaging for mapping bark beetle damage at tree-level. *Remote Sensing, 7*(11), 15467-15493.

Pearse, G. D., Morgenroth, J., Watt, M. S., & Dash, J. P. (2017). Optimising prediction of forest leaf area index from discrete airborne lidar. *Remote Sensing of Environment, 200*, 220-239.

Rhodes, M. W., Bennie, J. J., Spalding, A., ffrench-Constant, R. H., & Maclean, I. M. (2022). Recent advances in the remote sensing of insects. *Biological Reviews, 97*(1), 343-360.

Roussel, J.-R., Auty, D., Coops, N. C., Tompalski, P., Goodbody, T. R., Meador, A. S., Bourdon, J.-F., de Boissieu, F., & Achim, A. (2020). lidR: An R package for analysis of Airborne Laser Scanning (ALS) data. *Remote Sensing of Environment, 251*, 112061.

Senf, C., Seidl, R., & Hostert, P. (2017). Remote sensing of forest insect disturbances: Current state and future directions. *International journal of applied earth observation and geoinformation, 60*, 49-60.

Silva, C. R., Olthoff, A., de la Mata, J. A. D., & Alonso, A. P. (2013). Remote monitoring of forest insect defoliation. A review. *Forest Systems, 22*(3), 377-391.

St Peter, J., Drake, J., Medley, P., & Ibeanusi, V. (2021). Forest structural estimates derived using a practical, open-source lidar-processing workflow. *Remote Sensing, 13*(23), 4763.

Stone, C., Matsuki, M., & Carnegie, A. J. (2003). *Pest and disease assessment in young eucalypt plantations: field manual for using the Crown Damage Index*. Bureau of Rural Sciences.

Stone, C., Wardlaw, T., Floyd, R., Carnegie, A., Wylie, R., & De Little, D. (2003). Harmonisation of methods for the assessment and reporting of forest health in Australia—a starting point: A discussion paper prepared by a sub-committee of the Forest Research Working Group on Forest Health. *Australian Forestry, 66*(4), 233-246.

Vescovo, L., Gianelle, D., Dalponte, M., Miglietta, F., Carotenuto, F., & Torresan, C. (2016). Hail defoliation assessment in corn (*Zea mays L.*) using airborne LiDAR. *Field Crops Research, 196*, 426-437.

What is remote sensing? The definition guide. (2021, 07.12.21). GIS Geography. Retrieved 06.04.22, 2022, from https://gisgeography.com/remote-sensing-earth-observation-guide/

Ye, N., Morgenroth, J., Xu, C., & Chen, N. (2021). Indigenous forest classification in New Zealand–A comparison of classifiers and sensors. *International journal of applied earth observation and geoinformation, 102*, 102395.

APPENDICES

Table 1a: Multicollinearity above 0.95 between the existing metrics from the VUX-240 scanner from September 2021 (in total, 95 metrics).

Metric 1	Metric 2	Corr.	Metric 1	Metric 2	Corr.	Metric 1	Metric 2	Corr.
zmean	zwimean	0.999	zq45	zq55	0.977	zq45	zq60	0.965
zq65	zq70	0.997	zq75	zsqmean	0.977	zq20	zq30	0.965
zq80	zq85	0.996	zmean	zq50	0.977	zq60	zq75	0.964
zmean	zsqmean	0.996	zq70	zsqmean	0.976	zq40	zsqmean	0.964
zq85	zq90	0.995	zmax	zq95	0.976	zmax	zq90	0.963
zq40	zq45	0.995	zq15	zq20	0.975	zq55	zq70	0.962
zq75	zq80	0.995	zq35	zwimean	0.975	zq65	zwimean	0.962
zwimean	zsqmean	0.995	zq80	zsqmean	0.974	zq50	zq65	0.962
zq55	zq60	0.995	zq50	zsqmean	0.974	zq90	zsqmean	0.962
zq70	zq75	0.994	zq65	zsqmean	0.974	zq30	zimean	0.962
zq90	zq95	0.994	zmean	zq35	0.974	zq35	zq50	0.961
zq50	zq55	0.993	zq55	zq65	0.974	zmean	zq65	0.96
zq45	zq50	0.993	zq35	zimean	0.973	zmean	zq30	0.96
zq25	zq30	0.991	zq60	zsqmean	0.973	zq5	zq10	0.96
zq35	zq40	0.991	zq10	zq15	0.972	zq40	zq55	0.96
zq30	zq35	0.990	zq25	zq35	0.972	zq70	zwimean	0.96
zq60	zq65	0.990	zq55	zwimean	0.971	zmean	zq70	0.959
zq20	zq25	0.987	zq40	zimean	0.971	zq30	zwimean	0.959
zq80	zq90	0.986	zq45	zsqmean	0.971	zmean	zq75	0.957
zq75	zq85	0.985	zq75	zq90	0.971	zq75	zwimean	0.957
zq85	zq95	0.984	zwimean	zimean	0.971	zq30	zq45	0.956
zq65	zq75	0.984	zq80	zq95	0.970	zq35	zsqmean	0.955
zq50	zq60	0.983	zq55	zsqmean	0.970	zimean	zsqmean	0.954
zq45	zwimean	0.983	zq85	zsqmean	0.970	zq75	zq95	0.954
zq35	zq45	0.981	zq60	zwimean	0.969	zmean	zq80	0.953
zq70	zq80	0.981	zmean	zimean	0.969	zq95	zsqmean	0.952
zq50	zwimean	0.980	zq30	zq40	0.968	zq15	zq25	0.952
zq60	zq70	0.980	zmean	zq55	0.968	zq80	zwimean	0.952
zq40	zq50	0.980	zq65	zq80	0.967	zq50	zimean	0.951
zmean	zq45	0.980	zq45	zimean	0.966	zq50	zq70	0.951
zq40	zwimean	0.980	zmean	zq60	0.966	zmax	zq85	0.95
zmean	zq40	0.978	zq70	zq85	0.966			

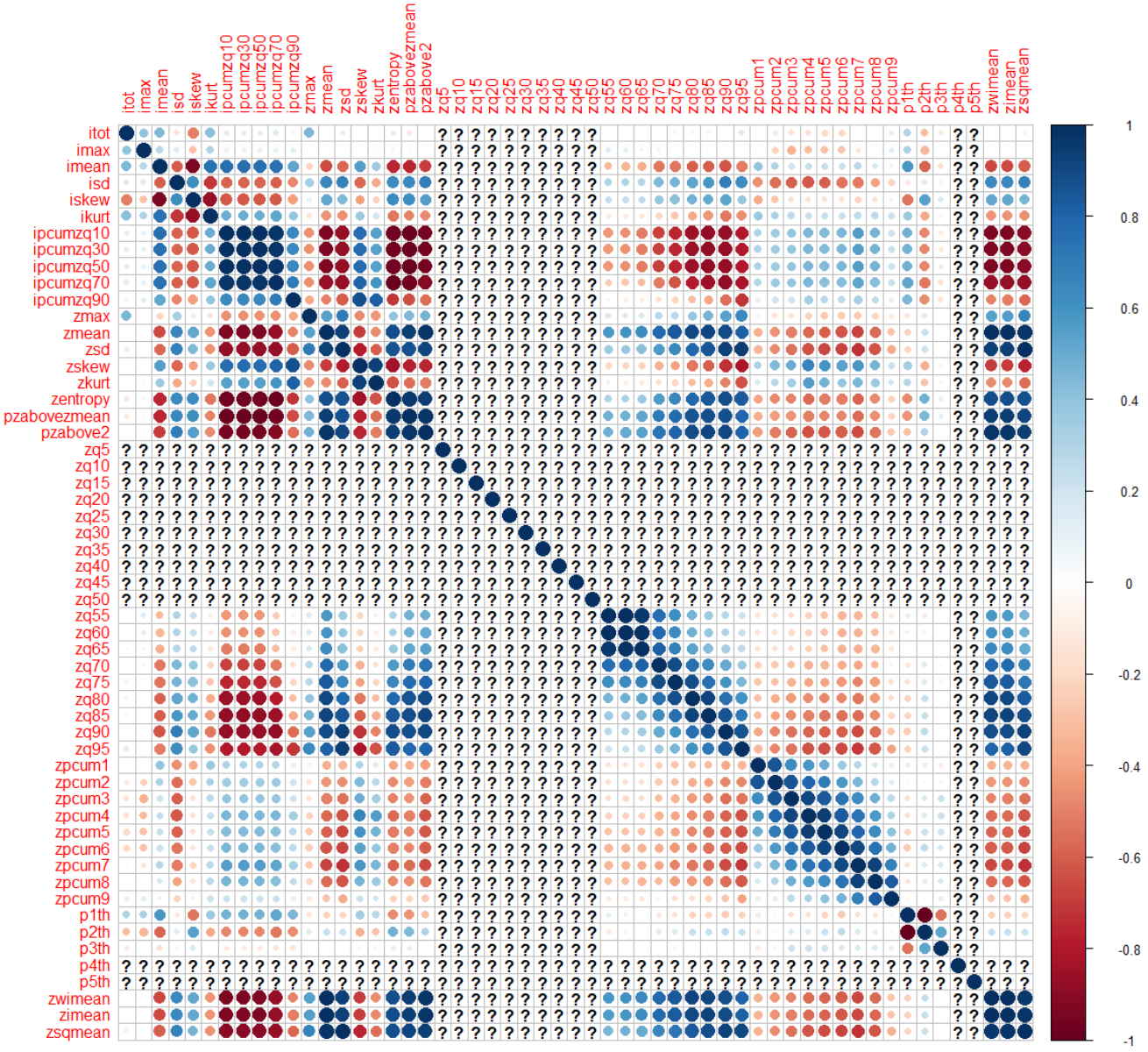

Figure 1a: Matrix correlation of the 57 different metrics for the VUX-1LR scanner from September 2021. Many metrics were highly correlated (model with multicollinearity), with 95 metric correlations above 0.95.

Table 2a: Multicollinearity above 0.95 between the existing metrics from the VUX-1LR scanner from September 2021 (in total, 33 metrics).

Metric 1	Metric 2	Corr.	Metric 1	Metric 2	Corr.	Metric 1	Metric 2	Corr.
ipcumzq10	ipcumzq30	1.000	ipcumzq50	pzabovezmean	-0.989	ipcumzq50	ipcumzq70	0.970
ipcumzq10	ipcumzq50	1.000	zq60	zq65	0.983	ipcumzq10	zentropy	-0.970
ipcumzq30	ipcumzq50	1.000	ipcumzq70	zentropy	-0.981	ipcumzq30	zentropy	-0.970
p1th	p2th	-1.000	pzabove2	zimean	0.973	ipcumzq50	zentropy	-0.970
zmean	zwimean	1.000	zmean	pzabove2	0.973	zq55	zq65	0.969
zmean	zimean	1.000	pzabovezmean	pzabove2	0.973	zentropy	pzabovezmean	0.969
zwimean	zimean	1.000	zimean	zsqmean	0.973	zwimean	zsqmean	0.967
zq55	zq60	0.998	pzabove2	zwimean	0.973	ipcumzq70	pzabovezmean	-0.963
zsd	zsqmean	0.993	zmean	zsqmean	0.971	ipcumzq10	pzabove2	-0.956
ipcumzq10	pzabovezmean	-0.989	ipcumzq10	ipcumzq70	0.970	ipcumzq30	pzabove2	-0.956
ipcumzq30	pzabovezmean	-0.989	ipcumzq30	ipcumzq70	0.970	ipcumzq50	pzabove2	-0.956

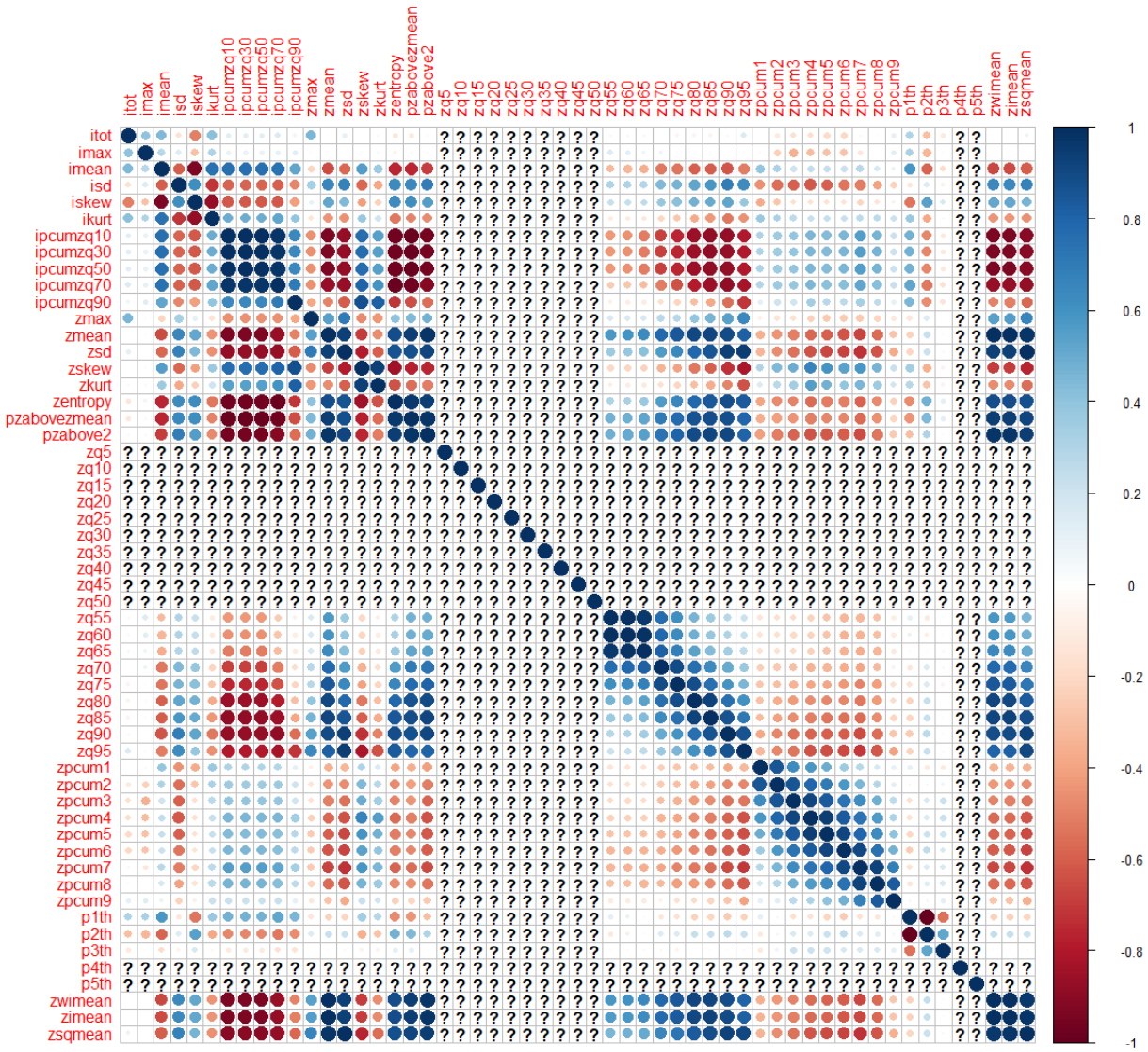

Figure 2a: Matrix correlation of the 57 different metrics for the VUX-1LR scanner from March 2022. Many metrics were highly correlated (model with multicollinearity), with 33 metric correlations above 0.95.

Table 3a: Multicollinearity above 0.95 between the existing metrics from the VUX-1LR scanner from March 2022 (in total, 33 metrics).

Metric 1	Metric 2	Corr.	Metric 1	Metric 2	Corr.	Metric 1	Metric 2	Corr.
ipcumzq10	ipcumzq30	1.000	ipcumzq50	pzabovezmean	-0.989	ipcumzq50	ipcumzq70	0.970
ipcumzq10	ipcumzq50	1.000	zq60	zq65	0.983	ipcumzq10	zentropy	-0.970
ipcumzq30	ipcumzq50	1.000	ipcumzq70	zentropy	-0.981	ipcumzq30	zentropy	-0.970
p1th	p2th	-1.000	pzabove2	zimean	0.973	ipcumzq50	zentropy	-0.970
zmean	zwimean	1.000	zmean	pzabove2	0.973	zq55	zq65	0.969
zmean	zimean	1.000	pzabovezmean	pzabove2	0.973	zentropy	pzabovezmean	0.969
zwimean	zimean	1.000	zimean	zsqmean	0.973	zwimean	zsqmean	0.967
zq55	zq60	0.998	pzabove2	zwimean	0.973	ipcumzq70	pzabovezmean	-0.963
zsd	zsqmean	0.993	zmean	zsqmean	0.971	ipcumzq10	pzabove2	-0.956
ipcumzq10	pzabovezmean	-0.989	ipcumzq10	ipcumzq70	0.970	ipcumzq30	pzabove2	-0.956
ipcumzq30	pzabovezmean	-0.989	ipcumzq30	ipcumzq70	0.970	ipcumzq50	pzabove2	-0.956

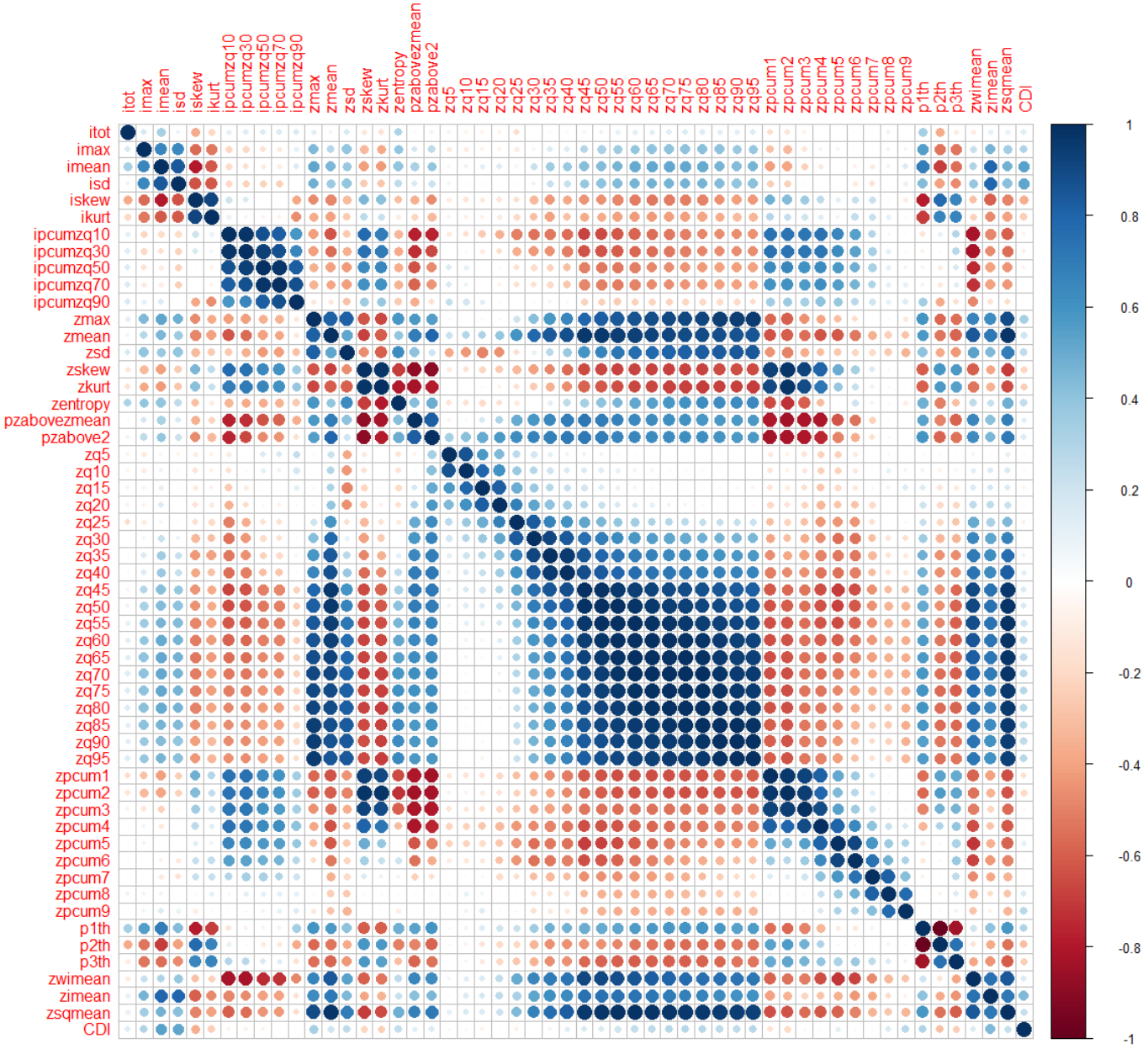

Figure 3a: matrix correlation of the 57 different metrics for the L1 scanner from March 2022. Many metrics were highly correlated (model with multicollinearity), with 54 metric correlations above 0.95.

Table 4a: Multicollinearity above 0.95 between the existing metrics from the L1 scanner from March 2022 (in total, 54 metrics).

Metric 1	Metric 2	Corr.	Metric 1	Metric 2	Corr.	Metric 1	Metric 2	Corr.
zq70	zq75	0.998	zq60	zq75	0.982	zq65	zq85	0.968
zq60	zq65	0.998	zq60	zsqmean	0.981	zq75	zsqmean	0.967
zq75	zq80	0.997	zq55	zsqmean	0.981	zq80	zq95	0.966
zq90	zq95	0.997	zkurt	zpcum2	0.980	zmean	zq45	0.964
zq65	zq70	0.996	zq70	zq85	0.979	zq55	zq75	0.963
zq55	zq60	0.993	zq65	zsqmean	0.977	zq75	zq90	0.963
zq85	zq90	0.993	zmean	zsqmean	0.977	zpcum1	zpcum2	0.961
zq70	zq80	0.993	zskew	zpcum2	0.976	zq80	zsqmean	0.961
zq50	zq55	0.992	zq50	zsqmean	0.976	zmean	zq50	0.960
zq65	zq75	0.991	zq55	zq70	0.974	zq50	zq65	0.960
zq80	zq85	0.991	zq50	zq60	0.974	zq45	zsqmean	0.960
zq60	zq70	0.990	zq70	zsqmean	0.973	zq75	zq95	0.959
zq45	zq50	0.990	zq60	zq80	0.972	zq70	zq90	0.957
p1th	p2th	-0.990	ipcumzq10	ipcumzq30	0.971	zq85	zsqmean	0.957
zq85	zq95	0.989	zskew	zkurt	0.971	zq60	zq85	0.957
zq55	zq65	0.985	ipcumzq50	ipcumzq70	0.970	zmax	zq95	0.954
zq75	zq85	0.985	zq80	zq90	0.970	zq35	zq40	0.954
zq65	zq80	0.983	zq45	zq55	0.969	zq70	zq95	0.953